

## PROBE MEASUREMENT ERRORS CAUSED BY SHEAR FLOWS

A. Appukuttan, R. J. Miller, H. P. Hodson

Whittle Laboratory  
University of Cambridge  
Cambridge, UK

### ABSTRACT

This paper reports the effect of shear flow on probe measurement errors. Measurement errors due to flow angle and velocity magnitude are investigated. The main causes of errors in shear flow are the apparent incidence angle that a probe experiences in shear flow and its interaction with the flow separation on probes. Three different geometries of probe are tested; a circular cylinder probe, a 45°-wedge probe and a 60°-wedge probe. Testing was conducted at engine representative probe Reynolds numbers.

When the probes were aligned with the flow, the measurement error in flow angle and velocity magnitude in all probes was mainly caused by the apparent incidence induced by the shear flow. When the probes were not aligned with the flow, the interaction of the shear flow with the flow separation around the nose of the probe dominated measurement errors. The errors in velocity magnitude and flow angle were quantified for the probe geometries investigated.

### 1. INTRODUCTION

Three or four sensor aerodynamic probes are widely used to measure flow angle, velocity and total pressure in turbomachinery environments. The measurements are often made in flows that contain velocity gradients, such as those that occur in wakes. The probes are calibrated in a uniform flow. The presence of shear flow can create a measurement error. Ideally, to ensure measurement accuracy in a shear flow, a probe should have a width that is at least an order of magnitude smaller than the half-width of the wake in which the measurement is made. However, this is often not possible either due to the type of measurement required or the extreme nature of the environment in which it is to be used. The first situation occurs when time-resolved measurements of an unsteady flow are required. The minimum size of the probe is then limited by the size of the fast-response silicon pressure transducers. The second situation occurs when measurements are required in engine

tests. The minimum size of the probe is then limited by cooling.

Ikui and Inoue (1970) experimentally tested a three-hole cobra probe. Their results showed that the error in flow angle measurement was a linear function of both the total pressure gradient of the shear and the separation of yaw pressure tappings. An empirical relation was derived using the yaw pressure coefficients and the dynamic pressures far upstream of each tapping. This method was found to accurately predict the measurement error. Dixon (1978) experimentally tested a sting mounted spherical probe and a wedge probe in a shear flow. He concluded that the error in flow angle measurement was a function of both the total pressure gradient of the shear and the spatial separation of yaw pressure tappings. Willinger and Haselbacher (2003) experimentally tested a three-hole cobra probe in a boundary layer. They concluded that the error in flow angle measurement was a linear function of the total pressure gradient of the shear. The results were explained using a projection method assuming each pressure tapping sees different flow conditions. The three papers do not report the effect of shear flow on velocity measurement error or the effect of changing the angle of the probe on measurement error.

Taylor (1917), Tsien (1943), Hall (1956) and Livesey (1956) used inviscid flow theory to investigate the effect of shear flow on the stagnation streamline upstream of the probe. The presence of shear was found to cause the stagnation streamline to bend away from the high velocity part of the shear as it approached the probe. This meant the streamline measured by the probe does not originate from a point directly upstream of the probe leading edge. The effect, known as 'streamline displacement' causes the stagnation streamline to approach the probe at an angle of incidence.

Hall (1956) reported that the effect of shear flow on the measurement error incurred by two-dimensional probes (e.g. wedge or cylinder) is very different to that incurred by three-dimensional probes (e.g. cobra and pyramid). In two-dimensional flow the vortex tubes remains constant

in strength and perpendicular to plane of shear. In three-dimensional flows the vortex tubes are stretched and bent as they pass around the probe leading edge. Hall found that this effect caused three-dimensional probes to have a larger 'streamline displacement' than two-dimensional probes.

The aim of the research reported in this paper is to investigate the effect of shear on measurement errors incurred by two-dimensional probes. Three geometries have been investigated, a 45° wedge, a 60° wedge and a circular probe. In the first part of the paper potential flow theory and numerical predictions were used to investigate the effect of linear shear flow on measurement error. In the second part of the paper large-scale models of the probes were tested in wake flows representative of those found in a turbomachine. The effects of linear shear flow were used to assess the experimental results in wake flow.

## NOMENCLATURE

a	radius of the infinite cylinder
$C_{ax}$	axial chord of a turbine blade
$C_{yaw}$	Yaw coefficient
$C_{tot}$	Total pressure coefficient
$C_{dyn}$	Dynamic coefficient
$C_p$	$(P - P_{s_{in}})/P_{dyn}$ at $y = 0$
$C_{p_{lin}}$	Pressure coefficient in a linear flow
D	Diameter of the probe
K	Non-dimensional velocity gradient
LE, TE	Leading edge and trailing edge of wedge probe
$P_0$	Pressure measured by the leading edge total pressure tapping
$P_1, P_2$	Pressure measured by the top and bottom yaw pressure tappings
$P_{0ref}$	Total pressure measured by pitot probe for reference
$P_{Sref}$	Static pressure measured by pitot probe for reference
$P_m$	$\frac{1}{2}(P_1 + P_2)$
$P_{0in}$	Total pressure at the inlet
$P_{dyn}$	Inlet dynamic pressure at $y = 0$
$P_\infty$	Static pressure at infinity
S	Distance of yaw pressure tapping from leading edge
$S_o$	Length of the side face of wedge probe
$\Delta u$	Difference between the reference and measured velocity magnitude by model probes
$U_o$	Free stream velocity at $y = 0$
$\Delta U$	Wake-depth at Loc-1 measured by reference probe
$U_{inf}$	Velocity far upstream from the center of wake
$U_y$	Undisturbed velocity at $y$ in a linear shear flow

x, y	Coordinate axis
X	Traverse position across the wake
$\alpha$	Flow angle
$\beta, \gamma$	Constants
r, $\theta$	Polar coordinate system
$\theta_{act}$	Actual flow angle across wake

## 2. EXPERIMENTAL AND NUMERICAL TECHNIQUES

The experiment set-up consisted of a test section placed at the exit of the wind tunnel as shown in Fig. 1. The test section had a cross-section of 685mm(height)×460mm(width) and a length of one meter. The shear flow was simulated using a wake generated by a circular bar fixed in the movable belt. The model probe was held fixed in the test section and the belt was moved using a stepper motor. The model probes were tested at different locations (Loc=1, 2, 3 and 4, see Fig. 1) downstream of the wake in order to investigate the influence of shear strength on the measurement error. At the tested locations the ratio of the distance between the location and the bar to the diameter of the bar was 16.5, 24.5, 32.5 and 40.5. The ratio of wake width to probe diameter corresponds to 2-3 mm probe traversing a trailing edge wake at 10-35%  $C_{ax}$  downstream of a HP turbine with a chord of 100 mm.

The model probe was also rotated by another stepper motor up to 20° through 5° interval, in order to study the influence upon different angles of attack.

The real velocity profile at all the four locations was measured using a miniature cobra probe (2 mm diameter). The error in velocity magnitude was calculated by dividing the deviation from the cobra probe data of the model probe data by the wake-depth at Loc = 1. The error in angle was calculated by subtracting the angle measured by the model probe data from the actual value (negligible across the wake, thus taken as zero).

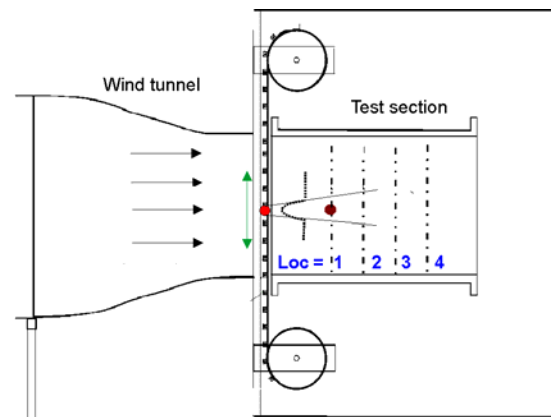


Fig. 1 Experimental set-up showing the probe and moving belt

For all cases tested, the inlet velocity at the working section was kept at  $12 \pm 0.5$  m/s. The Reynolds number based on the probe diameter was  $1.58 \times 10^4$  which is typical of the value encountered by using a 2-3 mm diameter probe in turbomachines.

Three different probe geometries were investigated. The velocity magnitude and flow angle were measured using the total pressure tapping located on the front and the yaw pressure tapping located on the sides of the probes. Fig. 2 shows the probe models and their dimensions. In the case of wedge probes the experiments were conducted for five different positions of yaw pressure tapping. In the case of the circular probes two different locations,  $30^\circ$  and  $60^\circ$  angular locations of yaw pressure tapping was investigated.

The probes were calibrated in the same test section with uniform flow. The measured turbulence intensity was less than 0.4%. The flow angle convention employed is shown in Fig. 3. The calibration coefficients are defined by (1)

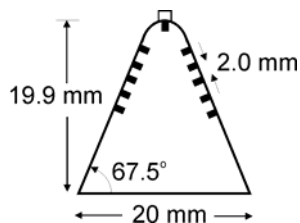
$$C_{yaw} = \frac{P_1 - P_2}{P_0 - P_m}$$

$$C_{dyn} = \frac{P_{0ref} - P_{sref}}{P_0 - P_m} \quad (1)$$

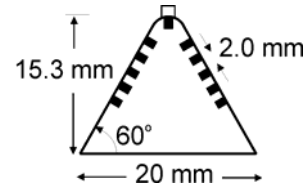
$$C_{tot} = \frac{P_{0ref} - P_0}{P_0 - P_m}$$

$$P_m = \frac{1}{2}(P_1 + P_2)$$

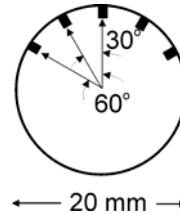
Numerical simulations were carried out using Fluent™ software to investigate measurement errors in linear shear flow. The segregated solver with second-order implicit in time and second-order upwinding for velocity discretization was used for all of the simulations using an unstructured grid. The geometry and boundary conditions are shown in Fig. 4. A linearly varying velocity profile was assigned at the inlet.



(a)



(b)



(c)

Fig. 2 Probe dimensions and pressure tapplings (a) 45°-wedge (b) 60°- wedge and (c) circular probe

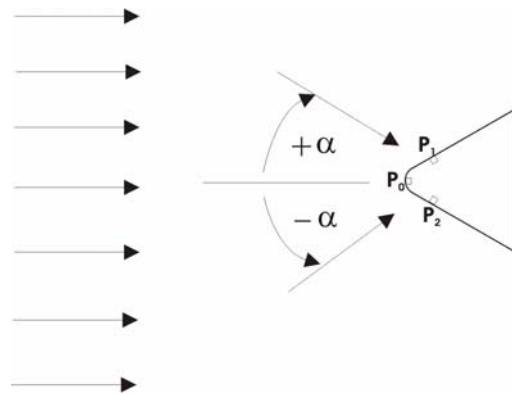


Fig. 3 Flow angle convention and yaw pressure tapplings in a 3-hole configuration

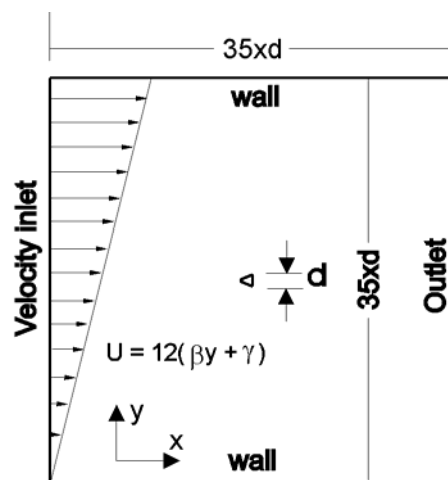


Fig. 4 Flow domain with linear velocity gradient at the inlet

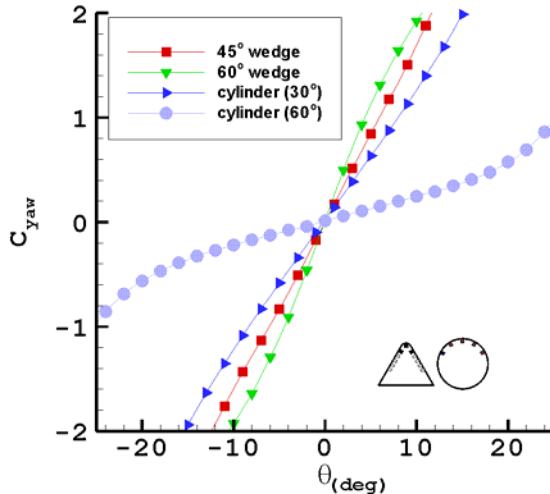


Fig. 5 Yaw coefficient curves for different probe geometries

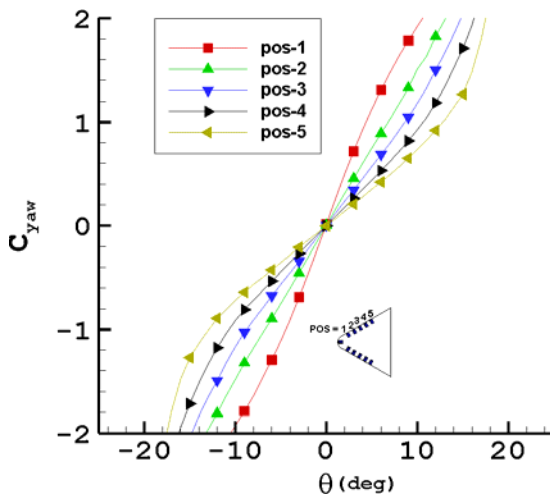


Fig. 6 Yaw coefficient curves for different positions of yaw pressure tapings in 60°-wedge.

### 3. PROBES IN UNIFORM FLOW

The yaw coefficient curve of all probes in uniform flow is discussed in this section. Fig. 5 shows the yaw coefficient curves for wedge probes (yaw pressure tapings placed near the leading edge) and circular probes (yaw pressure tapings at 30° and 60° from upstream stagnation point). It can be seen from the figure that the 60°-wedge probe showed the maximum slope of the yaw coefficient curve near the origin, among all the probe models investigated. For wedge probes, the slope near the origin was found to increase with apex angle (60° greater than 45°). In circular probes, placing pressure tapings close to the upstream stagnation point was found to increase the slope of yaw coefficient curve near the origin.

Fig. 6 shows the effect of moving the yaw pressure tapings on the slope of yaw coefficient curve near the origin of a 60°-wedge probe. The slope reduced with position of yaw pressure tapping. A similar

trend was also observed in 45°-wedge probe. Thus, it can be summarized that moving yaw pressure tapings away from the leading edge reduced the slope of yaw coefficient curve near the origin for all probe models.

### 4. LINEAR SHEAR FLOW

This section shows the effect of a linear shear flow on the surface pressure distribution around the cylindrical probes and wedge probes. The dimensionless strength of the shear flow approaching a probe of width  $a$  is given by  $K$

$$K = \frac{\partial U}{\partial y} \frac{a}{U_0} \quad (1)$$

where  $U$  is the velocity,  $y$  is the distance measured perpendicular to the flow direction and  $U_0$  is the upstream velocity on the center line of the probe. The findings from this section are then used to determine the suitability of the projection method, proposed by Willinger and Haselbacher (2003), for reducing the measurement errors caused by shear.

#### 4.1 Cylinder probes

The effect of linear shear on the inviscid flow field around a circular cylinder can be obtained analytically (Hall (1956)). If the velocity profile of the upstream shear flow is defined as

$$U = U_0 \left( 1 + K \frac{y}{a} \right) \quad (2)$$

then the stream function of the flow is given as

$$\psi = -U_0 \left( r - \frac{a^2}{r} \right) \sin \theta - \frac{U_0 K}{2} \frac{r^2}{a} \sin^2 \theta - \frac{U_0 K}{4} \frac{a^3}{r^2} \cos 2\theta \quad (3)$$

The first term is the solution for a uniform flow past a cylinder. The second term adds a shear flow to the free stream. The third term can be seen as the effect of an image vortex inside the cylinder.

The path of the stagnation streamline in a linear shear flow is determined by the balance of the second and third terms in equation 3. Far upstream, term 2 dominates while close to the cylinder; term 3 becomes greater than term 2. This causes the stagnation streamline to bend towards the lower velocity part of the shear, and results in an incidence angle,  $\alpha$ , onto the probe. This is shown in Fig. 7. This effect also causes a vertical displacement,  $\delta$ , in the stagnation streamline. This effect was investigated by Taylor (1917), Tsien (1943), Hall (1956) and Livesey (1956) and is known as the displacement effect.

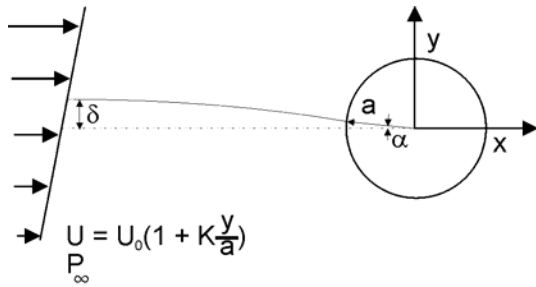


Fig. 7 Schematic of a cylinder in a linear shear flow

The variation of incidence angle of the stagnation streamline,  $\alpha$ , with the strength of shear  $K$  can be determined from the locus of the stagnation streamline. Equation 3 then becomes

$$U_0 a \sin \alpha = \frac{U_0 K a}{4} \cos 2\alpha \quad (4)$$

and for small angles this becomes

$$\sin \alpha = \frac{1}{4} K \quad (5)$$

For small angles, the incidence of the stagnation streamline onto the probe is determined only by the dimensionless strength of the upstream shear. The analytical inviscid solution and two computational solutions are plotted in Fig. 8. The shaded region represents the range of typical values of  $K$  experienced by a 3mm probe in a turbomachine, which is calculated from the shear flow in a trailing edge wake of a HP turbine blade.

The above analysis shows the effect of shear flow on the stagnation streamline. To understand the effect of shear flow on probe measurement error it is necessary to understand the effect of shear flow on the pressure coefficient around the whole probe. Fig. 9 shows the pressure coefficient around the probe with and without shear flow.

The shear reduces the pressure coefficient on the bottom of the probe while increasing it on the top. This results in the cylinder having lift. An incidence change onto a cylinder does not result in lift and therefore incidence alone cannot explain the change in the pressure field.

The higher pressure coefficient around the top of the probe is the result of the increased upstream velocity in the shear. The increased momentum of this fluid requires a larger force to deflect it around the cylinder.

The pressure coefficients in Fig. 9 can be used to determine the angle error that occurs when a cylinder probe is placed in a linear shear flow. The calibration coefficients used are given in equation 1. The variation in angle measurement error over a range of shear strengths,  $K$ , and a range of yaw pressure tapping positions is shown in Fig. 10.

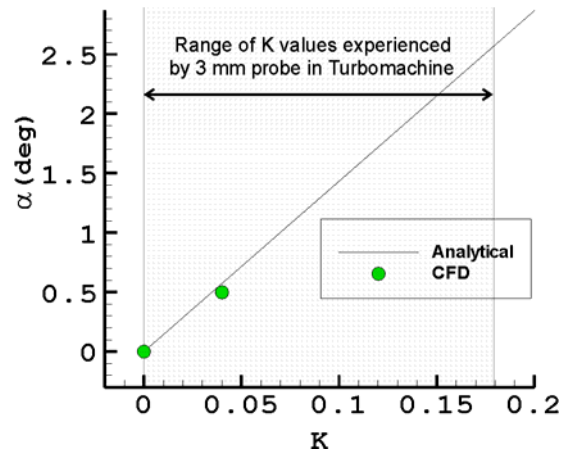


Fig. 8 Incidence of stagnation streamline in linear shear flow for a cylinder probe.

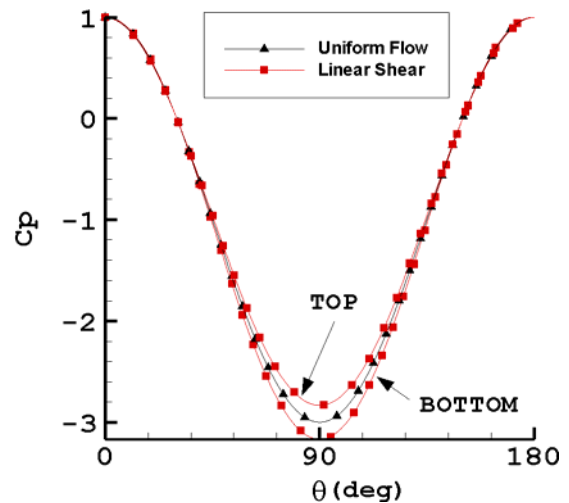


Fig. 9 Pressure coefficient in uniform and linear shear flow for a cylinder probe

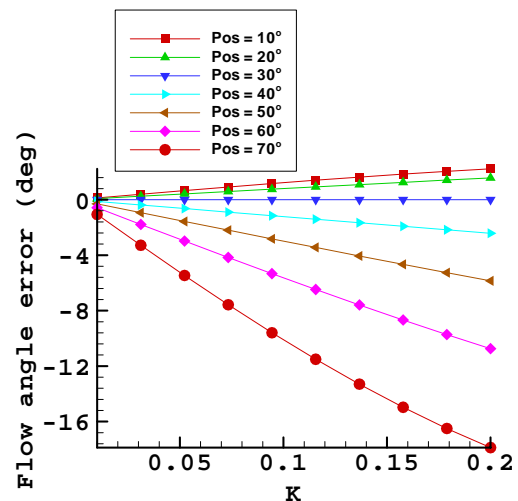


Fig. 10 Flow angle error in linear shear flow for a cylinder probe

For a fixed position of the yaw pressure tappings the error can be seen to increase almost linearly

with  $K$ . It is interesting to note that when yaw pressure tappings are located at  $30^\circ$  the probe incurs no error in the measured flow angle. For a fixed value of  $K = 0.1$ , the error in flow angle increased from  $2^\circ$  to  $-10^\circ$  when moving yaw pressure tappings from  $10^\circ$  to  $70^\circ$  angular locations. It should be noted that this is only for a cylinder probe in an inviscid flow. For a viscous flow the potential field of the wake results in a change in the angle of yaw pressure tappings at which minimum measurement error occurs.

#### 4.2 Wedge probes

The effect of a linear shear on the flow field around a wedge probe was determined using a time-resolved viscous numerical prediction. Solutions were obtained for two wedges with leading edge angles of  $45^\circ$  and  $60^\circ$ . The shear strength was set at  $K=0.028$ . The time-resolved solution resolved the vortex shedding from the probe trailing edge. The results presented in this section were time-averaged over one vortex-shedding period.

Fig. 11 shows the pressure contours around the  $60^\circ$  wedge probe. The stagnation point can be seen to have moved towards the top surface of the probe. This is caused by the stagnation streamline bending towards the lower velocity part of the shear and is the same phenomena as observed in the cylinder probe. The stagnation streamline was found to have an incidence angle  $\alpha=10^\circ$  on the leading edge circle of the wedge. This compares to a cylinder in the same strength of shear flow having  $\alpha=0.4^\circ$ .

To understand the effect of shear flow on probe measurement error it is necessary to understand the effect of shear flow on the pressure coefficient around the whole probe. Fig. 12 shows the pressure coefficient around the  $60^\circ$  wedge probe shown in Fig. 11. The pressure coefficient for the same wedge probe in uniform flow with an incidence angle of  $2.65^\circ$  is also shown.

The difference in pressure coefficient across the probe caused by linear shear was found to be very close to that caused by incidence alone. The difference in  $\Delta C_p$  between a linear shear of  $K=0.028$  and an incidence of  $2.65^\circ$  was found to be less than 5% of  $C_p$  in linear shear flow. This shows that the wedge probe has a very different behaviour in shear flow than a cylinder probe. It is interesting to note that the stagnation streamline was found to have an incidence of  $10^\circ$ .

The pressure coefficient for a wedge probe with a  $45^\circ$  leading edge angle is shown in Fig. 13. The same strength of shear was used as in Fig. 12. The minimum pressure coefficient is higher than for the  $60^\circ$  wedge. Linear shear was found to change the

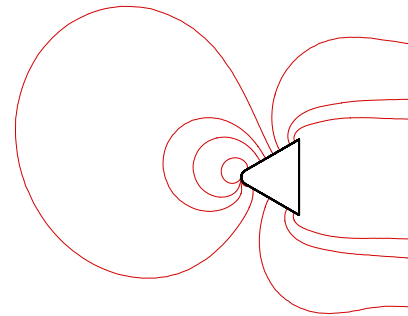


Fig. 11 Pressure contours around the  $60^\circ$  wedge in a linear shear flow

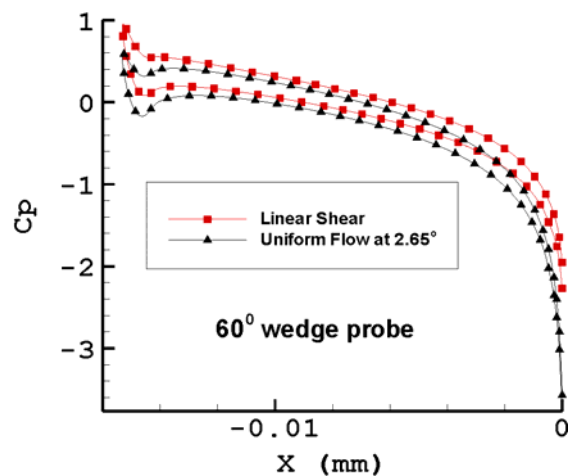


Fig. 12 Pressure coefficient on  $60^\circ$  wedge probes in linear shear

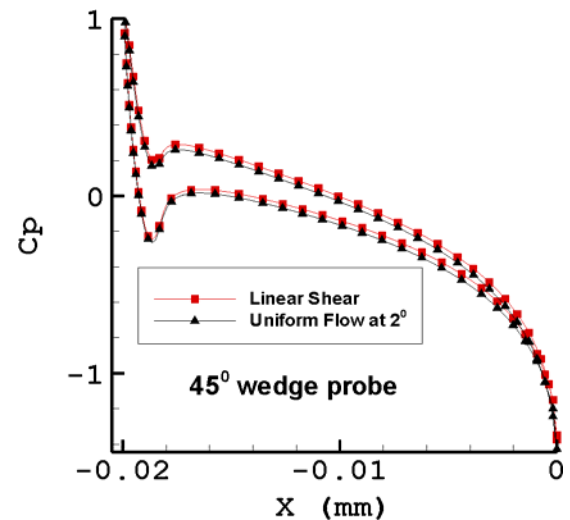


Fig. 13 Pressure coefficient on  $45^\circ$  wedge probes in linear shear

pressure coefficient in the same way as for the  $60^\circ$  wedge. The incidence angle that corresponded to a shear of  $K=0.028$  was  $2^\circ$ , which is lower than the value of  $2.65^\circ$  for a  $60^\circ$  wedge.

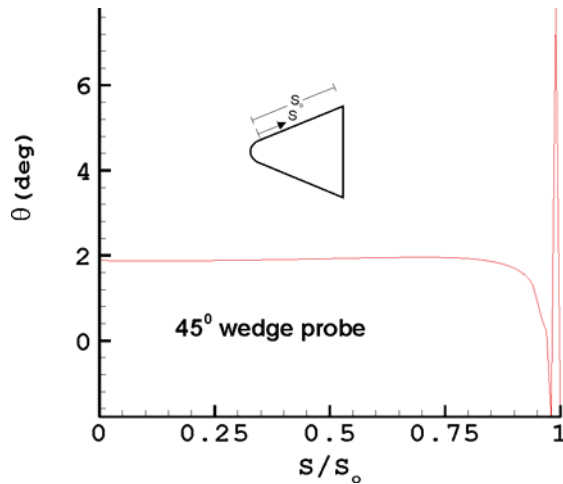


Fig. 14 Flow angle error in linear shear flow for 45°-wedge probe

The pressure coefficients in Fig. 13 can be used to determine the angle error that occurs when a 45° wedge probe is placed in a linear shear flow. The calibration coefficients used are given in equation 1. The variation in angle measurement error for a shear strength of  $K=0.028$  for different positions of yaw pressure tapping is shown in Fig. 14. As expected the results show that the flow angle is constant with different positions of yaw pressure tapping.

#### 4.3 Error compensation

A number of papers have proposed methods of compensating probes for errors that occur in shear flows. These include both Ikui and Inoue (1970) and Willinger and Haselbacher (2003). Most methods involve the assumption that the pressure measured by each tapping of the probe originates from a streamline at a location directly upstream; this is the basis of the projection method.

To test how accurately the projection method compensates the pressure coefficient for linear shear, the pressure coefficient for uniform flow was plotted against the compensated pressure coefficient (Fig. 15). If each tapping were to see a different streamline, then the result will be a line of unity gradient passing through origin. The results for a cylinder in inviscid flow show this behaviour. The line is invariant of shear strength,  $K$ , and shows that the streamline projection method accurately compensates for measurement error in shear flow. The results for the wedge probe show a line of changing gradient that does not pass through the origin. The line is found to move with the strength of shear,  $K$ . This shows that for wedge probes the simple projection method does not accurately compensate the probe for measurement error.

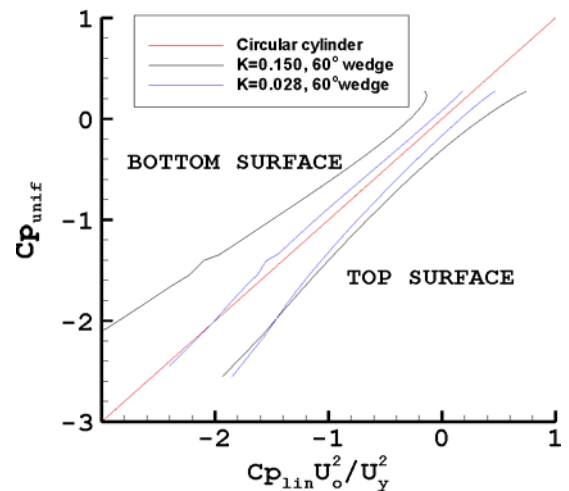


Fig. 15 Relation between  $C_p$  in linear flow and uniform flow for cylinder and 60° wedge probes

### 5. PROBES IN A WAKE FLOW

In this section, the measurement errors caused by a wake flow representative of those found in turbomachines are investigated. The wake flow is simulated using a circular bar. Each probe was tested at four locations downstream of the bar. The real velocity of wake, flow angle and pressure distribution across the wake was measured using a small cobra probe. The velocity profile of the wake at each location is shown in Fig. 16. The shaded region in the plot corresponds to region with high gradients in velocity at location 1. This will be marked on all future figures. The variation in shear strength,  $K$ , across the wake is shown in Fig. 17. The magnitude of the shear strength can be seen to peak at each side of the wake and return to zero in the middle.

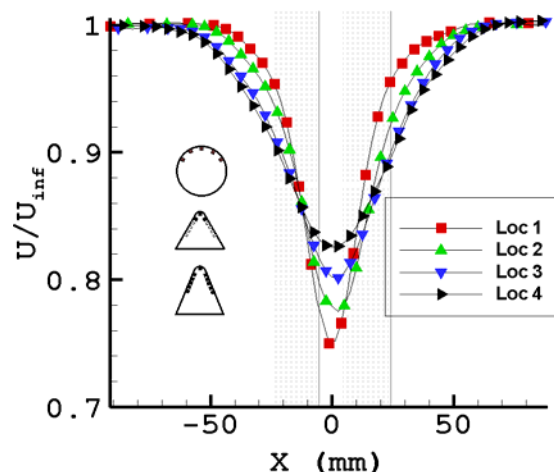


Fig. 16 Velocity profile across the wake at different locations downstream measured by cobra probe

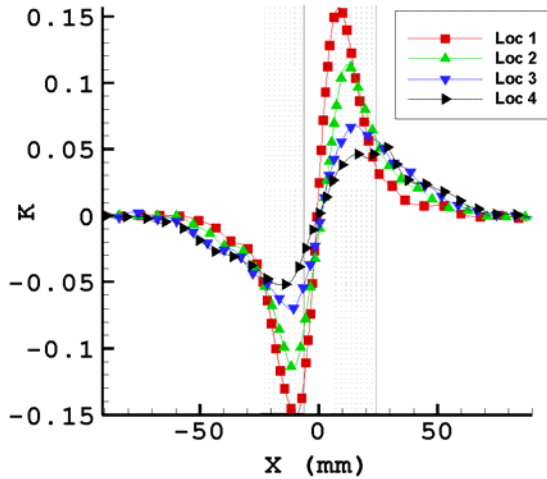


Fig. 17 The non-dimensional velocity gradient,  $K$  across the wake at different locations downstream measured by cobra probe

The following section is split into five parts the first two parts reports the error in angle measurement with the probe mounted both in upstream flow direction and at incidence. The third and fourth part reports the error in velocity measurement with the probe mounted both in upstream flow direction and at incidence. The last part discusses the optimum probe geometry and location of yaw pressure tappings that incurs minimum error in wake flow.

### 5.1 Flow angle error at zero angle of attack

The error in flow angle measurement at zero angle of attack caused by wake flow is discussed in this section. Fig. 18 shows the measurement error at different locations downstream of the bar for a circular probe with yaw pressure tappings at  $30^\circ$ . The variation of angle error was very similar to the variation of  $K$ . At different locations downstream, the error followed the trend of  $K$ . A similar profile was also observed in wedge probes but the peak error was different (see Fig. 19). The circular probe (yaw pressure tappings at  $30^\circ$ ) showed maximum error in flow angle followed by  $60^\circ$ - wedge probe and  $45^\circ$ - wedge probe.

Fig. 20 shows the error in flow angle with  $K$  across the wake at different locations for a circular probe (yaw pressure tappings at  $30^\circ$ ). It shows that the angle error increases almost linearly with  $K$ . A comparison of the variation of angle measurement error with  $K$  for all probes is shown in Fig. 21. The results show that probe models exhibited a linear trend of error with  $K$ , with circular probes exhibiting maximum flow angle error.

The variation of flow angle error with position of yaw pressure tappings is plotted in Fig. 22. In the case of the circular probe (Fig. 22a) the error did

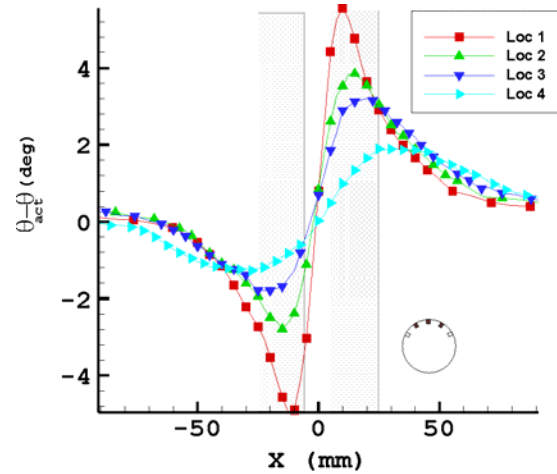


Fig. 18 Flow angle errors across the wake at different locations for a circular probe with yaw pressure tappings at  $30^\circ$ .

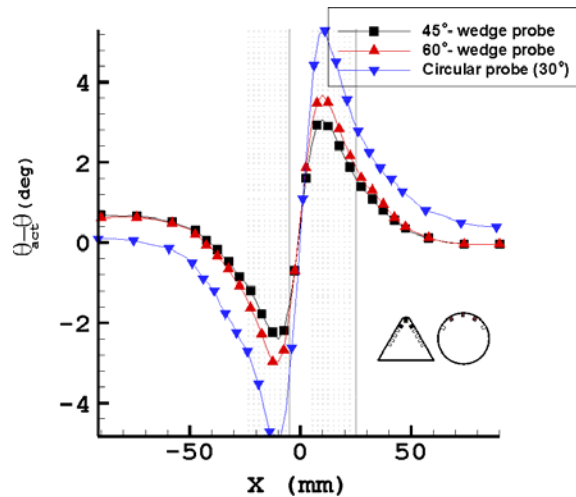


Fig. 19 Errors in flow angle across the wake for all probe models at  $Loc = 1$ .

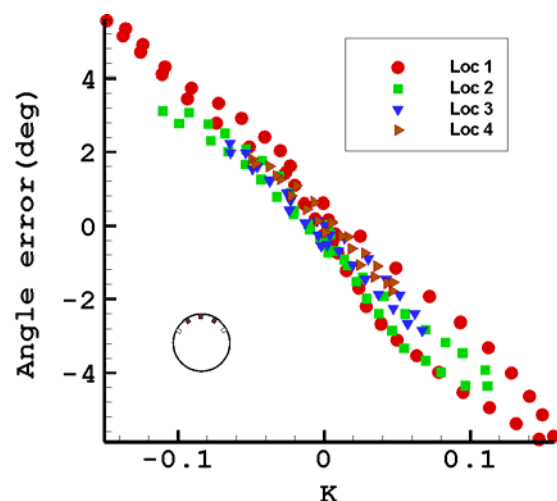


Fig. 20 Errors in flow angle for circular probe ( $30^\circ$ )

not vary when the yaw pressure tappings were moved from  $30^\circ$  to  $60^\circ$  angular locations. This did not agree with linear shear flow investigation presented in section 4.1.

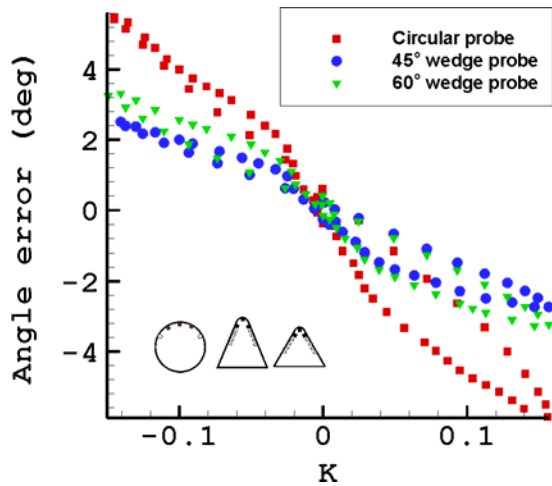
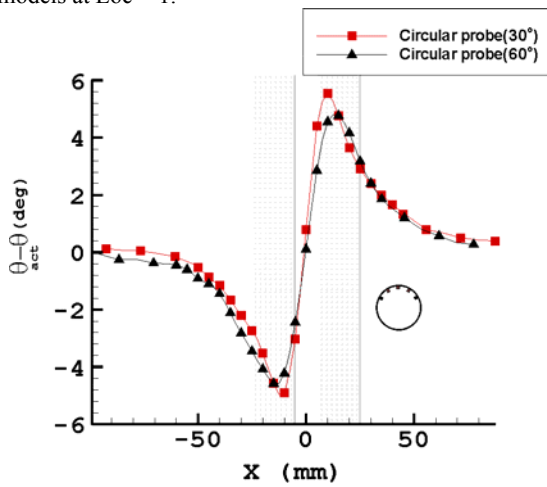
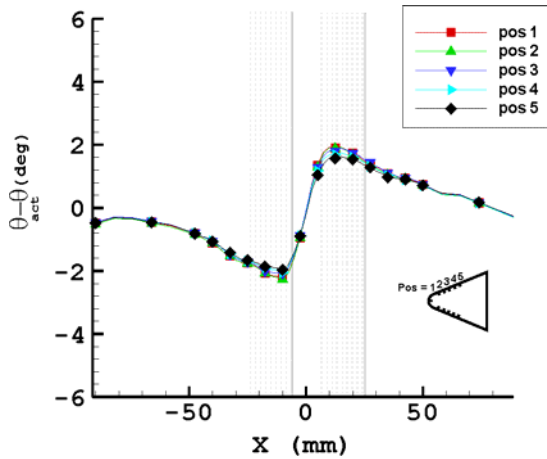


Fig. 21 Errors in flow angle across the wake for all probe models at Loc = 1.



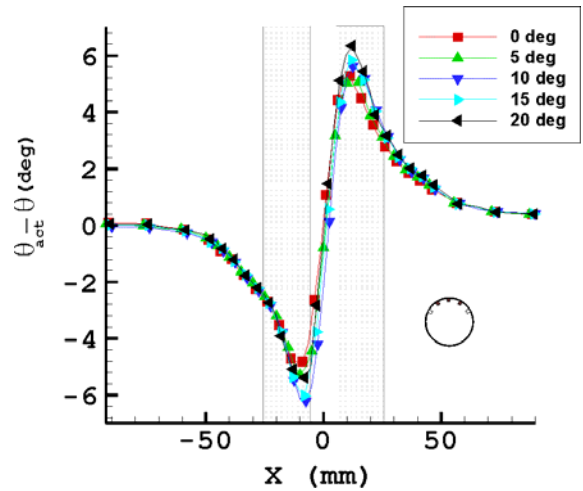
(a)



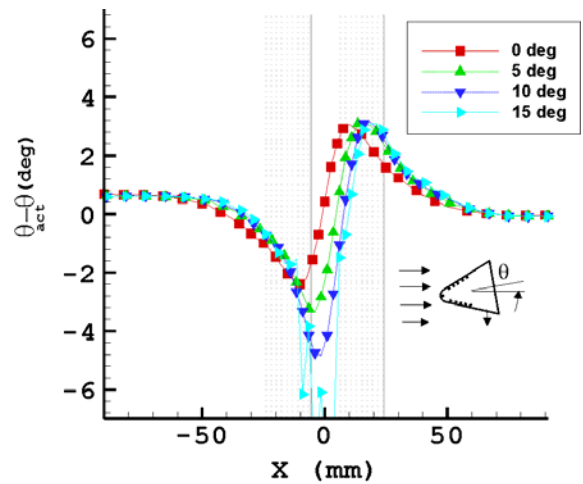
(b)

Fig. 22 Errors in flow angle for different yaw pressure tappings at Loc = 1 (a) circular probe and (b) 45°-wedge probe

A linear shear flow predicted no error in angle measurements for yaw pressure tappings at 30° and a high error for yaw pressure tappings at 60°. The



(a)



(b)

Fig. 23 Measurement error in flow angle at different angles of attack (a) circular probe (30°) and (b) 45°-wedge at Loc = 1.

disagreement is likely to be caused by viscous phenomena and requires more investigation. In the case of 45°-wedge probe (Fig. 22b) the error did not vary with the position of yaw pressure tapping (with variations less than 0.4°). This was in agreement with the results of linear shear flow (see section 4.2), which showed that wedge probes experience an apparent global incidence. In this case, viscous effects were included in the analysis.

## 5.2 Flow angle error at incidence

The measurement error at incidence was computed by turning the probe through 20° at 5° intervals. Fig. 23 shows the variation of error at incidence. The circular probe with yaw pressure tappings at 30° did not show any variation of angle error with incidence (Fig. 23a). In the case of wedge probes, the error was observed to rise with incidence (Fig. 23b). Above 10° incidence, a very large error was

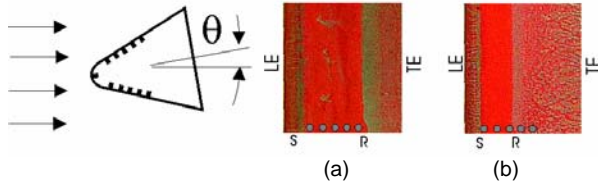


Fig. 24 Oil flow visualization experiments showing the leading edge separation bubble on the upper face of the 45°-wedge probe at 10° incidence for (a) uniform flow and (b) wake flow (higher velocity on the upper face).

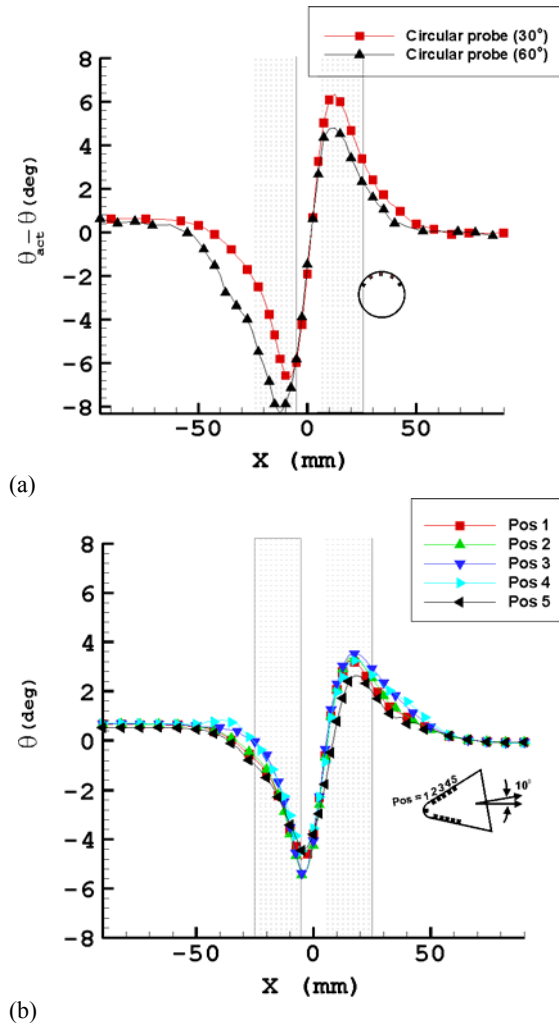


Fig. 25 Measurement errors in flow angle at 10° incidence at Loc = 1 (a) Circular probe and (b) 45°-wedge probe

observed. A leading edge separation bubble was observed above 10° incidence on the wedge probes. Fig. 24a shows the separation bubble near the leading edge of 45°-wedge probe at 10° incidence in uniform flow. In the wake flow, the interaction of the shear with the separation bubble moved the reattachment line towards (depending on the sign of the shear) the leading edge as shown in Fig. 24b.

This altered the pressure distribution and caused high measurement errors

The variations of flow angle error with the position of the yaw pressure tapings at 10° incidence is plotted in Fig. 25. For circular probes, Fig. 25a shows that the error was found to increase when moved the yaw pressure tapings from 30° to 60°. The higher error at 60° may be due to the proximity of the yaw pressure tapings to the flow separation during incidence. It is known that the separation point in the circular probes oscillates at the vortex shedding frequency. The mean location of the separation point moves towards or away from the upstream stagnation point in the presence of shear. This phenomenon may significantly affect the yaw pressure tapings at 60° during incidence but not at 30°. Fig. 25b shows the variation of flow angle error with the position of the yaw pressure tapings for a 45°-wedge probe. There was not much change observed in angle error with the position of the yaw pressure tapping. A similar trend was observed in 60°-wedge probe.

### 5.3 Velocity error at zero angle of attack

The error in velocity measurement at zero angle of attack caused by wake flow is discussed in this section. Fig. 26 shows the velocity measurement errors across the wake at all locations for a 60°-wedge probe with yaw pressure tapings near the leading edge. It can be seen from the figure that the measurement error increased towards the center of wake, peaking in the high shear domain with a slight reduction of error in the zero-shear region. It should be noted that the error did not reduce to zero at the center of wake where  $K = 0$ . This is because of the comparable size of the probe to the wake half-width. The magnitude of error was found to show a small drop with location of measurement plane. This is very different from the trend of angle error shown in Fig. 18.

Fig. 27 shows the measurement error in velocity magnitude at first location (Loc=1) for all probe models at zero angle of attack (in wedge probes, the yaw pressure tapings at pos = 1). The error peaked in the maximum shear domain for all probes and showed a reduction in error at the wake center. This clearly shows that the velocity error is a function of  $K$  but not a linear function as flow angle error, as it did not show zero error at the center of the wake (where  $K = 0$ ) for all locations investigated. The 60°-wedge probe showed maximum error in velocity followed by 45°-wedge probe and circular probe.

The variation of velocity error with the position of the pressure tapings is shown in Fig. 28. For the circular probe the measurement errors for yaw tapings at 30° and 60° were similar outside the

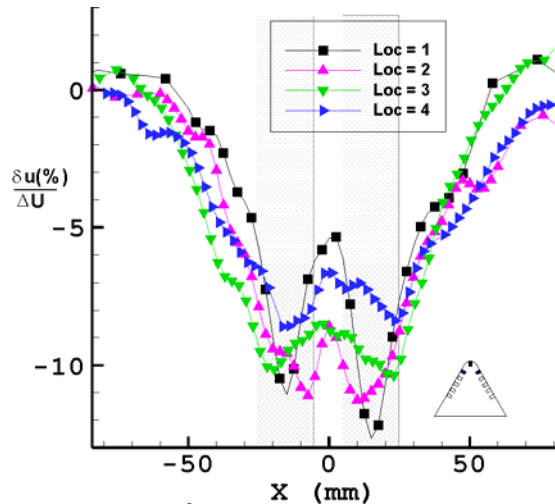


Fig. 26 Error in 60°-wedge probe at different locations

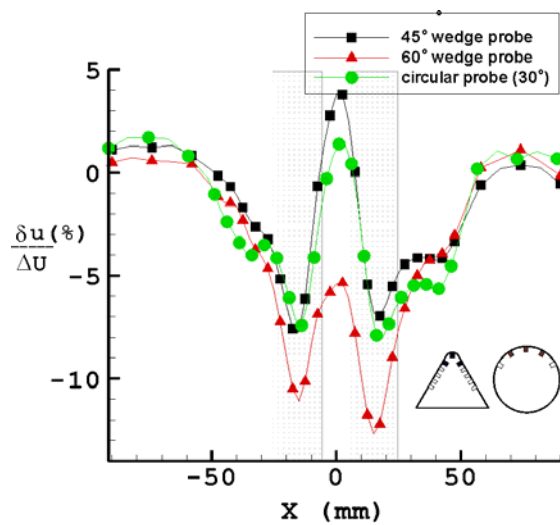
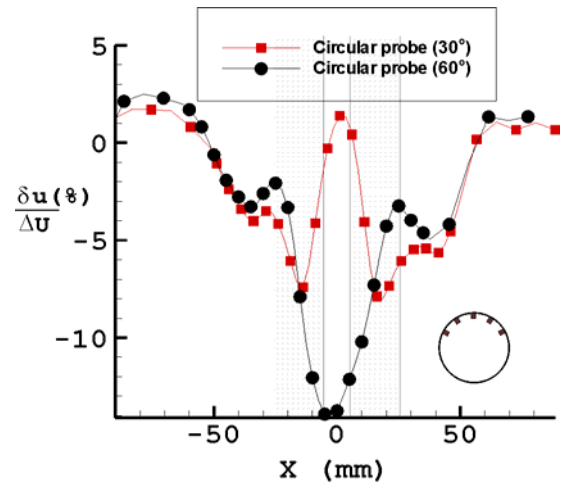


Fig. 27 velocity measurement error for all probe models at Loc=1

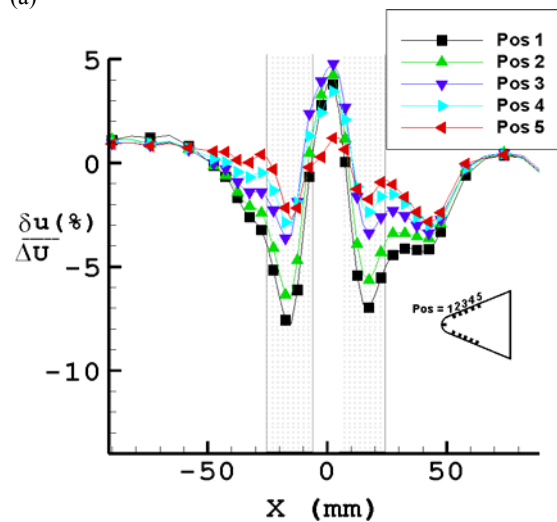
center of wake. At the center of wake, a large error was observed for yaw pressure tapplings at 60°. This may be due to the high spatial separation of yaw pressure tapplings at 60°. The yaw pressure tapplings at 60° are 8.67 mm from the probe centerline. Fig. 17 shows that at this location each yaw pressure tapping is in a region with high shear on the opposite sides of the wake. This results in high velocity measurement error. In the case of 45°-wedge probe (Fig. 28b), the error reduced with the position of yaw pressure tapping. The minimum error occurred for rearmost yaw pressure tapping (pos=5). Similar trend was also noted for the 60°-wedge probe. The reason for this trend is not yet understood.

#### 5.4 Velocity error at incidence

The measurement error at incidence was computed by turning the probe through 20° at 5° intervals. Fig. 29 shows the variation of error at incidence. The circular probe with yaw pressure tapplings at 30° did not show much variation of velocity error



(a)

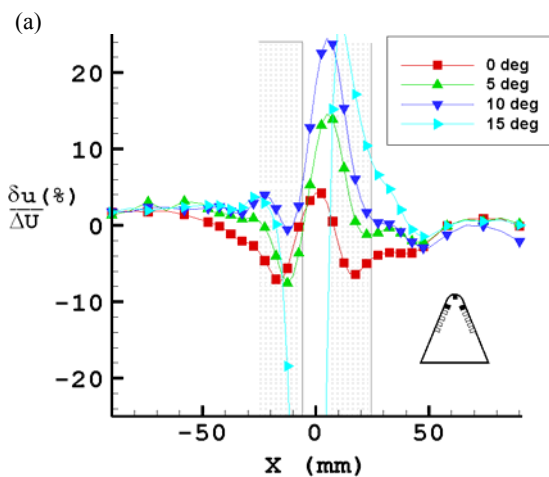
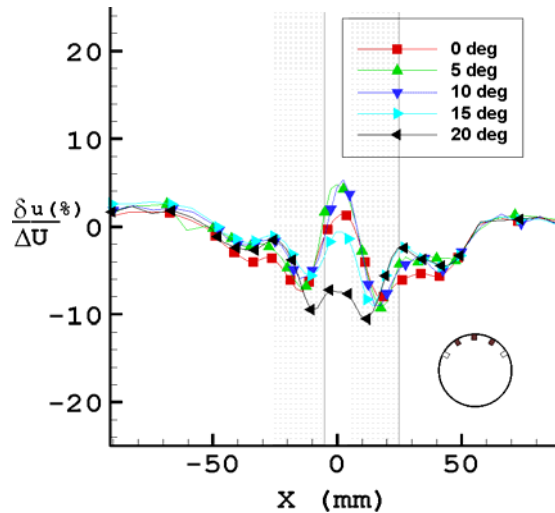


(b)

Fig. 28 velocity measurement error at different yaw pressure tapplings at Loc=1 (a) circular probe (b) 45°-wedge probe.

in the maximum shear (shaded region in the figure) region of the wake flow with incidence as shown in Fig. 29a. In the case of 45°-wedge probe (Fig. 29b), the error increased rapidly with inclination. The rise in error was caused by the interaction of the shear with the leading edge separation bubble (see section 5.2). In Fig. 29b, the results are only presented up to 15° incidence, since the error was beyond the defined range at 20° incidence. The trend in error incurred by the 60°-wedge probe was similar but smaller than 45°-wedge probe. This is due to the smaller separation bubble on the 60°-wedge probe.

The variations of error with the position of yaw pressure tapplings at 10° incidence is plotted in Fig. 30. For the circular probe, the error increased when moving the yaw pressure tapplings to 60°. This may be due to the interaction of the shear flow with the flow separation and the pressure tapplings' proximity to flow separation during incidence as explained in section 5.2. In the case of 45°-wedge



(b)

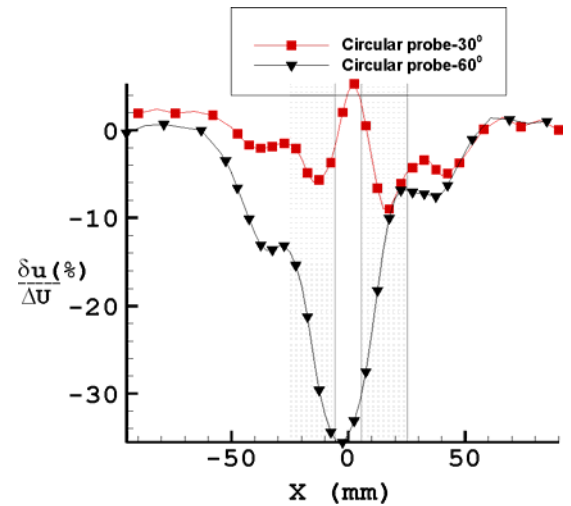
Fig. 29 Measurement error in velocity magnitude at different angles of attack at Loc = 1 (a) circular probe-30° (b) 45°-wedge probe

probe, the error increased rapidly from leading edge yaw pressure tapping (pos=1) to third position (pos=3). Then, it decreased with position of yaw pressure tapping. This is due to the pressure tapping's proximity to reattachment line of the separation bubble. It can be seen from Fig. 24 that the wake flow changes the reattachment line of separation bubble from fifth pressure tapping (pos=5) to third tapping (pos=3).

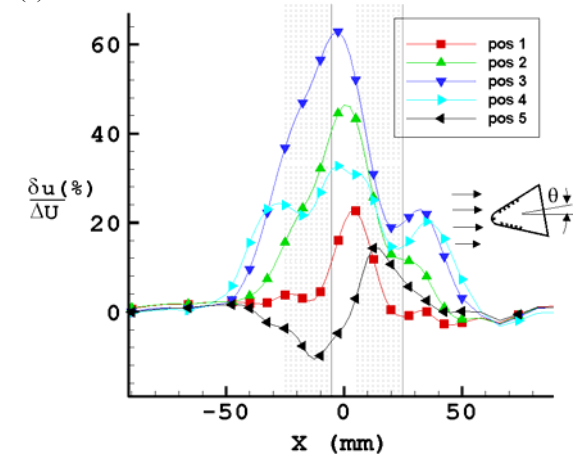
### 5.5 Choice of probe and position of yaw pressure tappings

This section summarizes the previous results and discusses the selection of probe geometry and the optimum location of yaw pressure tappings based on the results from the wake flow experiments.

Fig. 31 shows the maximum errors in flow angle measurements for all probe geometries at Loc = 1 with different positions of yaw pressure tappings. In the cases of wedge probes (Fig. 31a and b), the error increased with incidence. For different



(a)



(b)

Fig. 30 Measurement error in velocity magnitude with different yaw pressure tappings for 10° incidence at Loc = 1 (a) circular probe (b) 45°-wedge probe

positions of yaw pressure tapping, the error was almost a constant up to 15° incidence. The error increased with apex angle of the wedge probe, but at an incidence greater than 10° the error was larger for the smaller apex angle. For the 45°-wedge probe with yaw pressure tappings near the leading edge (pos = 1), the maximum error increased from 2° to 9° when the probe was inclined up to 15° (see Fig. 31a) and for the 60°-wedge probe, it increased from 3° to 6°.

Fig. 31c shows that the maximum error in flow angle measurements for the circular probe was almost insensitive to incidence for yaw pressure tappings at 30°. For yaw pressure tappings at 60°, the error increased with incidence due to the proximity of tappings to the flow separation. At incidences from zero up to 15°, the error increased from 5.3° to 5.7° for yaw pressure tappings at 30° and from 4.5° to 6.7° for yaw pressure tappings at 60°.

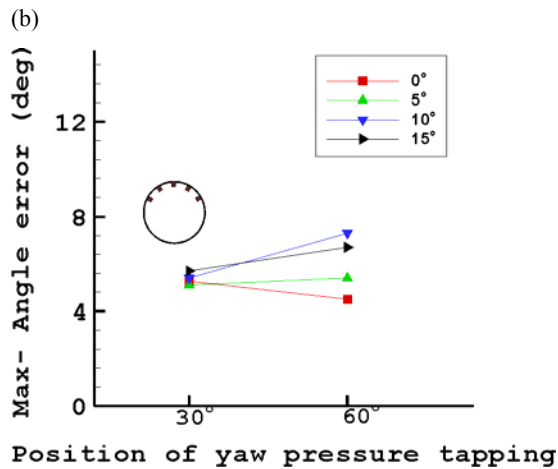
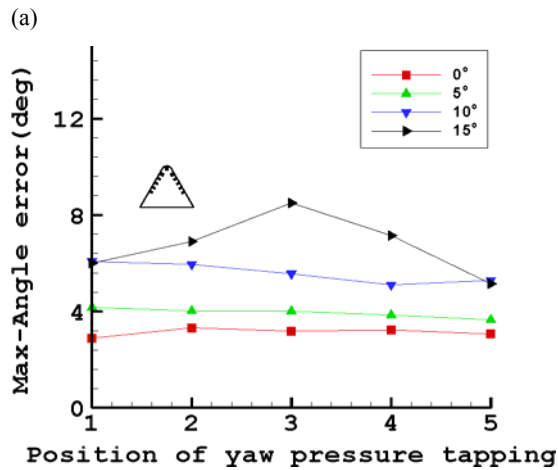
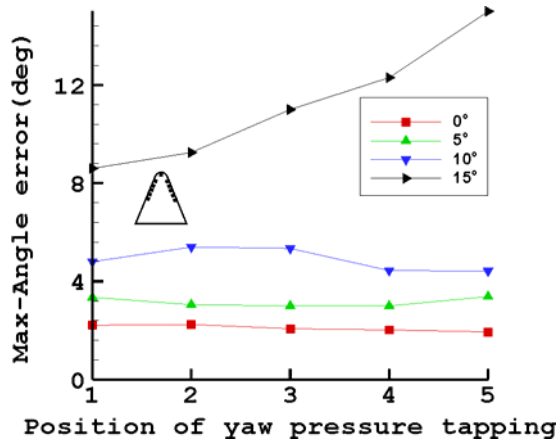


Fig. 31 Maximum error in angle measurements at Loc = 1 in (a) 45°-wedge and (b) 60°-wedge and (c) circular probe.

The trend in velocity measurement error was more complex. There was a high dependence on the location of the yaw pressure tapings. Fig. 32 summaries the maximum velocity error for all probes at different incidence angles with different positions of the yaw pressure tapping. In the cases of wedge probes (Fig. 32a and b), the minimum error in velocity measurements was observed for leading edge (pos=1) or rear mounted yaw pressure

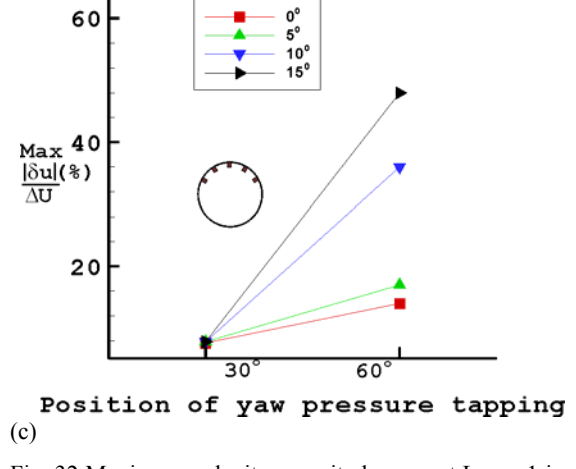
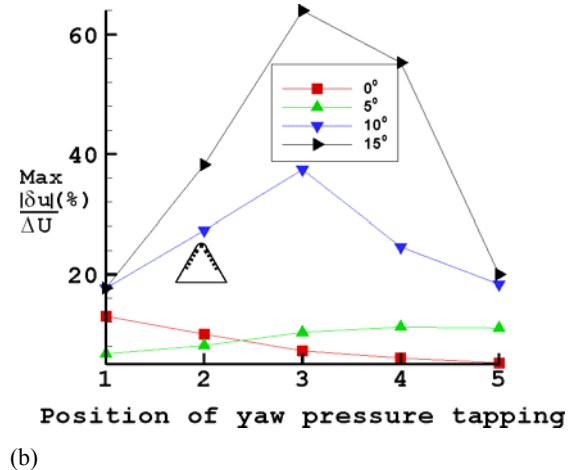
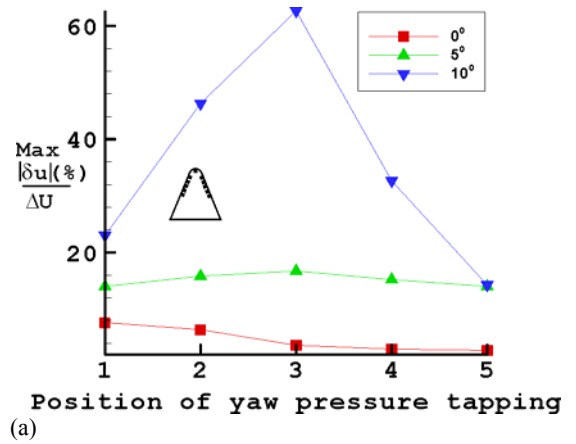


Fig. 32 Maximum velocity magnitude error at Loc = 1 in (a) 45°-wedge and (b) 60°-wedge and (c) circular probe.

tappings (pos=5) at all incidences. For other yaw pressure tapping positions, pos=2,3,4, the error increased to values higher than 25% at incidences above 10°. This is due to the pressure tapings' proximity to the reattachment line of the separation bubble in shear flow (see section 5.4). In Fig. 32a, the errors are plotted only up to 10° incidence since large errors occurred above this angle. It can be seen from Fig. 32a that the 45°-wedge probe was more accurate at zero angle of attack with the rear mounted yaw pressure tapings (pos=5). With the rear mounted yaw pressure tapings, the error in

velocity measurements increased from 3% to 14% when the probe was inclined up to 10°. Fig. 32b shows that the 60°-wedge probe was more accurate at zero degree angle of attack with yaw pressure tappings at leading edge (pos=1) or at trailing edge (pos=5). With rear mounted yaw pressure tappings, the error in velocity measurements increased from 5% to 20% when the probe was inclined from zero up to 15°.

The circular probe with yaw pressure tappings at 30° (Fig. 32c) had errors of less than 5% in velocity magnitude at all angles investigated. For the pressure tappings at 60°, the error increased from 14% to 48%.

Based on the above findings, it can be concluded that of the probe geometries tested in this paper, the circular probe with yaw pressure tappings at 30° has the lowest measurement error.

## CONCLUSIONS

Using linear shear flow, it has been shown that cylinders and wedges are affected by shear in a very different way. For cylinders, the shear flow caused a rise in pressure coefficient on the top surface and a displacement of upstream stagnation point. Incidence alone could not explain these phenomena. For wedge probes, the shear flow caused an apparent global incidence onto the probe. Also, the displacement of upstream stagnation point on wedges was found to be higher than that measured for cylinder. The apparent incidence angle due to shear flow was higher in the case of 60°-wedge probe than 45°-wedge probe.

In engine representative wake flows, cylinder probes did not agree with the inviscid linear shear flow model. The disagreement was due to the viscous effects i.e. flow separation and vortex shedding. For wedge probes, the angle error predicted by CFD with a linear shear flow agreed with the results of wake flow. At incidences above 10°, the interaction of the shear flow with the leading edge separation bubble caused very high flow angle errors. The velocity errors in wake flows are more complex. The shear flow interaction with the flow separation at the rear in circular probes and the shear flow interaction with leading edge separation bubble on wedge probes caused very high errors in velocity measurement.

## ACKNOWLEDGMENTS

This work was sponsored by Cambridge Commonwealth Trust and Nehru Trust (India). The authors would like to thank the technicians in the Whittle laboratory.

## REFERENCES

- Dixon, S. L., 1978, "Measurement of flow direction in a shear flow", *J. Phys, E:Sci. Instrum.*, **Vol.11**. pp 31-34
- Hall, I. M., 1956, "The displacement effect of a sphere in two-dimensional shear flow", *J. Fluid Mechanics*, **1**, pp 493-512.
- Ikui, T., Inoue, M., 1970, "Pressure or Velocity Gradient Error in the Flow Direction Measurement", *Memoirs of the faculty of Engineering Kyushu University*, **Vol. 29**, No. 3, pp, 121-136.
- Livesey, H. J. L., 1956, "The behavior of transverse cylindrical and forward facing total pressure probes in transverse total pressure gradient", *J. Basic. Eng*, **23**, pp 949-955.
- Taylor, Sir G. I. 1917, "Motion of solids in fluids when the flow is not irrotational", *Proceedings Royal Society*, **A93**, 99-114.
- Tsien, H. S., 1943, "Symmetrical Zhukovski airfoils in shear flow", *Quarterly applied mathematics*, **1**, 130-148. (Th.). 15.
- Willinger, R., Haselbacher H., 2003, "A Three-Hole Pressure Probe Exposed to Velocity Gradient Effects-Experimental Calibration and Numerical Investigation", *Conference of Modelling Fluid Flow (CMFF'03), The 12<sup>th</sup> International Conference on Fluid Flow Technologies*, Budapest, Hungary, Sept 3-6.